RSC Advances

PAPER

View Article Online
View Journal | View Issue

Cite this: *RSC Adv.*, 2025, **15**, 21401

Mechano-responsive color changes of a Pt(II) complex possessing triethylene glycol towards pressure sensors†

Masaya Yoshida,‡[ab] Takehiro Hirao,‡[a] Shin-ichi Kihara*[c] and Takeharu Haino *[ab]

Received 27th March 2025
Accepted 17th June 2025

DOI: 10.1039/d5ra02152a

rsc.li/rsc-advances

Mechanochromic molecules have attracted significant attention owing to their potential in the development of pressure sensors. However, relatively few studies have investigated the detailed mechanisms of the mechano-responsive nature and the quantitative visualization of mechanical forces. Herein, we report a square-planar platinum complex possessing triethylene glycol chains that exhibits mechanocromic behavior in the amorphous phase. Its mechanochromic nature was established using a combination of spectroscopic techniques, powder X-ray diffraction analyses, and computational chemistry techniques. The continuous changes in emission intensity allowed the platinum complex to be used as a mechanical force sensor, where the output signals were readable using a luminescence spectrometer. These findings demonstrate the potential benefits of square-planar platinum complexes and triethylene glycol chains for the creation of mechanochromic material.

Introduction

A remarkable feature of mechanochromic molecules is their ability to manifest unique mechano-responsive properties that can visualize mechanical forces to be changes in absorption and emission colors, which allows for the production of pressure sensors and data storage carriers.[1–6] Mechano-responsive properties have been determined to result from alterations in molecular bonds or supramolecular structures induced by mechanical forces.[7–22] To date, the vast majority of studies on mechanochromic molecules have demonstrated qualitative color changes in response to mechanical forces.[23] Thus, aside from a quantitative discussion of the mechanisms of color change, there remains a pivotal requirement for additional mechanochromic molecules that can quantitatively visualize mechanical forces. Recently, a few studies investigated mechanochromic molecules that can be used to quantitatively visualize the mechanical forces within polymer films.[24–29] Accordingly, it is worth developing mechanochromic molecules capable of quantitatively visualizing mechanical forces to expand their scope.

Square-planar platinum(II) complexes exhibit strong luminescence emissions from a metal-to-ligand charge transfer (MLCT) excited state.[30] Appropriately designed square-planar platinum(II) complexes form self-assembled constructs through intermolecular Pt–Pt and/or π–π stacking interactions, resulting in luminescence emission from a metal–metal-to-ligand charge transfer (MMLCT) excited state.[31,32] The emission color of the assembled platinum(II) complexes is determined by the Pt···Pt distance;[33,34] accordingly, the energetic inputs generating Pt···Pt distance changes afford emission color change of the platinum complexes.[4,10,35–51] In light of these reports, we envisage that Pt complex-based mechanochromic molecules would display continuous changes in their emission color or intensity in response to mechanical forces, leading to mechanical force sensors being used as analytical tools.

Our group previously reported the self-assembly of neutral platinum(II) complexes possessing isoxazole moieties to form supramolecular assemblies in various solvents.[52–57] Within these reports, we documented that the absorption and emission colors of the platinum(II) complexes were significantly altered by the solvent polarity, concentration of the platinum complexes, and solution temperature. The changes in absorption and emission colors were observed as a result of changing the Pt···Pt distance within the assembled structure. Therefore, the Pt···Pt distance of our platinum(II) complex may be altered by the application of mechanical forces. Herein, we report a square-planar platinum complex possessing a triethylene glycol (TEG) side-chain **1** that exhibits mechanochromic behavior with near-infrared emission, which is rarely reported

[a]*Department of Chemistry, Graduate School of Advanced Science and Engineering, Hiroshima University, 1-3-1 Kagamiyama, Higashi-Hiroshima, Hiroshima 739-8526, Japan. E-mail: haino@hiroshima-u.ac.jp*

[b]*International Institute for Sustainability with Knotted Chiral Meta Matter (SKCM²), Hiroshima University, 1-3-1 Kagamiyama, Higashi-Hiroshima, Hiroshima 739-8526, Japan*

[c]*Department of Chemical Engineering, Graduate School of Advanced Science and Engineering, Hiroshima University, 1-4-1 Kagamiyama, Higashi-Hiroshima, Hiroshima 739-8527, Japan. E-mail: snkihara@hiroshima-u.ac.jp*

† Electronic supplementary information (ESI) available. See DOI: https://doi.org/10.1039/d5ra02152a

‡ These two authors contributed equally.

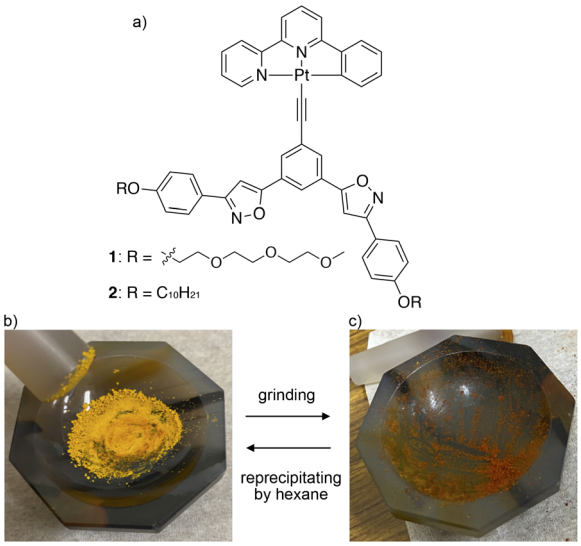

Fig. 1 (a) Molecular structure of platinum complex **1** possessing TEG chains and **2** possessing decyl chains. Optical images of mechanically (b) unground ($\mathbf{1}_{unground}$) and (c) ground ($\mathbf{1}_{ground}$) powders of **1** showing the color change induced by the mechanical force.

(Fig. 1a). In addition, the investigation of the mechanochromic behavior of **1** revealed the key role of the oligo-ethylene oxide chains in the emergence of its mechano-responsive nature. Thus, the following findings help to deepen our understanding of mechano-responsive molecules.

Experimental

General

All solvents were commercial reagent grade and were used without further purification. Luminescence and excitation spectra were measured using a JASCO FP-6500 spectrometer. Infrared (IR) spectra were recorded on a JASCO FT/IR-4600 spectrometer. PXRD patterns were measured using Smart Lab (Rigaku Inc.) with Cu Kα radiation ($\lambda = 1.5418$ Å) at a scanning rate of 2.0° min^{-1}, an applied voltage of 40 kV, and a current of 50 mA. NMR spectra were recorded on a Bruker APEX 400 MHz and Ascend 700 MHz spectrometers. Chemical shifts are quoted as parts per million (ppm) relative to residual chloroform (δ = 7.26 and 77.0 for ^{1}H and ^{13}C, respectively). Differential scanning calorimetry (DSC) analysis was conducted on a SEIKO instrument Inc., EXSTAR6000 (DSC6200 TG/DTA6200). The DSC curves were recorded at a heating rate of 15 °C min^{-1}. Melting points were determined using a Yanagimoto micro melting point apparatus, which were uncorrected. ESI-Mass spectra were reported with a Thermo Fisher Scientific LTQ Orbitrap XL. Elemental analyis was performed on a Perkin-Elmer 2400II elemental analyzer. Recycling preparative GPC-HPLC separations were carried out on a JAI LC-5060 system using preparative JAIGEL-2.5HH and 2HH columns in series. Previously synthesized **1** was used in this study; purity data and detailed experimental procedures are provided in our previous paper.[55]

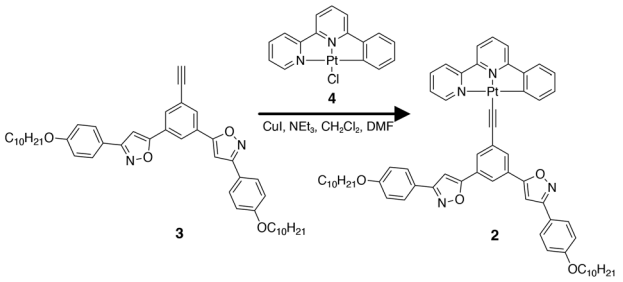

Scheme 1 Synthesis of platinum complex **2**.

Synthesis of complex 2

To a solution of **3** (120 mg, 0.17 mmol) and (6-phenyl-2,2′-bipyridine)platinum (**4**) chloride (80 mg, 0.17 mmol) in dry CH_2Cl_2 (13 mL) and dry DMF (8 mL) was added dry NEt_3 (190 μL, 0.9 mmol). The resulting solution was deoxygenated by bubbling nitrogen for 30 min, and then CuI (7 mg, 3 μmol) was added. After being stirred at room temperature for 21 h under an argon atmosphere in the dark, the reaction mixture was quenched with a portion of water. The resulting mixture was extracted with CH_2Cl_2. The organic layer was washed with saturated aqueous NaCl, dried over anhydrous Na_2SO_4, and concentrated in *vacuo*. The residue was separated by column chromatography on silica gel (5% methanol in CH_2Cl_2, eluent), followed by the purification using gel permeation chromatography to give the desired product **2** (101 mg, 53%) as an orange solid (Scheme 1): m.p. 265–268 °C; ^{1}H NMR (700 MHz, $CDCl_3$): δ 9.24 (d, 1H, J = 4.7 Hz), 8.08 (s, 1H), 8.06 (s, 2H), 8.05 (d, 1H, J = 7.0 Hz), 7.98 (d, 1H, J = 7.4 Hz), 7.90 (d, 1H, J = 8.0 Hz), 7.84–7.80 (m, 5H), 7.62–7.60 (m, 2H), 7.56 (d, 1H, J = 8.0 Hz), 7.37 (d, 1H, J = 7.4 Hz), 7.23 (t, 1H, J = 6.8 Hz), 7.09 (t, 1H, J = 6.8 Hz), 7.00 (d, 4H, J = 8.4 Hz), 6.89 (s, 2H), 4.02 (t, 4H, J = 6.6 Hz), 1.82 (m, 4H), 1.48 (m, 4H), 1.37 (m, 4H), 1.34–1.26 (m, 20H), 0.89 (t, 6H, J = 7.1 Hz) ppm; ^{13}C NMR (176 MHz, $CDCl_3$) δ 169.4, 165.8, 162.7, 160.7, 158.0, 154.5, 151.8, 146.7, 141.8, 138.9, 138.8, 138.5, 131.7, 130.5, 130.4, 128.2, 128.0, 127.7, 124.6, 124.0, 122.5, 121.3, 119.4, 118.5, 117.5, 114.9, 109.5, 104.9, 98.0, 77.2, 77.0, 76.8, 68.1, 31.9, 29.6, 29.6, 29.4, 29.3, 29.2, 26.0, 22.7, 14.1 ppm; HRMS (ESI^+) calcd for $[C_{62}H_{66}N_4O_4Pt + H]^+$ m/z 1126.48048, found m/z 1126.47930; anal. calcd for $C_{62}H_{66}N_4O_4Pt$: C 66.0, H 5.91, N 4.97, found C 65.84, H 5.83, N 4.87%.

Results and discussion

Synthesis and mechanochromic behaviors

The platinum complex **1** was synthesized according to the synthetic pathway described previously.[55] **1** was dissolved in dichloromethane (DCM), and hexane was added to the resulting solution, yielding a yellow precipitate ($\mathbf{1}_{unground}$, Fig. 1b). $\mathbf{1}_{unground}$ exhibited a discernible color change from yellow to red upon grinding the powder of $\mathbf{1}_{unground}$ using a mortar and pestle ($\mathbf{1}_{ground}$, Fig. 1c). During the grinding process, $\mathbf{1}_{ground}$ became stickier compared to $\mathbf{1}_{unground}$. The dissolve-in-DCM then reprecipitate-by-hexane process allowed a color change of

$\mathbf{1}_{\mathbf{ground}}$ from red-to-yellow, indicating that $\mathbf{1}_{\mathbf{ground}}$ reverted back to the original $\mathbf{1}_{\mathbf{unground}}$. Notably, no discernible changes in the ^{1}H NMR spectra were observed between the spectra of yellow-colored powder $\mathbf{1}_{\mathbf{unground}}$ and red-colored powder $\mathbf{1}_{\mathbf{ground}}$ in $CDCl_3$ (Fig. S1†). These results indicate that the color change originated from neither a chemical reaction nor molecular decomposition; therefore, the molecular arrangement of **1** in the solid state was primarily responsible for the color change.

Characterization of the luminescence

To determine the emission colors of **1**, the solid-state emission spectra of $\mathbf{1}_{\mathbf{unground}}$ and $\mathbf{1}_{\mathbf{ground}}$ were monitored. Based on our previous report,[55] **1** showed characteristic absorption band at 444 nm in solution; thus, the solution-phase emission spectra were recorded at an excitation wavelength of 444 nm within the work. According to the absorption band of **1**, the solid-state emission spectrum $\mathbf{1}_{\mathbf{unground}}$ was recorded at an excitation wavelength of 444 nm. $\mathbf{1}_{\mathbf{unground}}$ showed an emission band at approximately 570 nm with a quantum emission yield (Φ) of 3.4% (Fig. 2, black line). In contrast, emission bands at approximately 700 nm ($\Phi = 2.7\%$) and 570 nm were observed in the emission spectrum of $\mathbf{1}_{\mathbf{ground}}$ (Fig. 2, red line). In light of our previous study, the emission band at approximately 700 nm was ascribed to the MMLCT emission band derived from Pt–Pt interactions. This observation suggests that the mechanical grinding induced the reorientation of the packing structures of **1** in the solid state, resulting in the molecular arrangement with an appropriate Pt⋯Pt distance to promote intermolecular Pt–Pt interactions. Further support for the MMLCT emission was provided by the excitation spectra of $\mathbf{1}_{\mathbf{unground}}$ and $\mathbf{1}_{\mathbf{ground}}$. The excitation spectrum of $\mathbf{1}_{\mathbf{unground}}$ ($\lambda_{em} = 568$ nm) corroborated that the emission band at approximately 570 nm was derived primarily from the absorption band at approximately 444 nm, which is characteristic of π–π* and MLCT transitions[52] (Fig. 2, dotted black line). In contrast, the excitation spectrum of $\mathbf{1}_{\mathbf{ground}}$ ($\lambda_{em} = 710$ nm) clearly showed a characteristic MMLCT-absorption band (approximately 535 nm[52]), which supports the Pt–Pt interactions between molecules (Fig. 2, dotted red line). To further research the mechanochromic behavior of **1**, the solid-state emission spectra of platinum complexes possessing decyl side chains **2** (Fig. S2†) were monitored. No apparent changes in the luminescence band were observed, indicating that the TEG chains played a central role in the mechanochromic behavior.

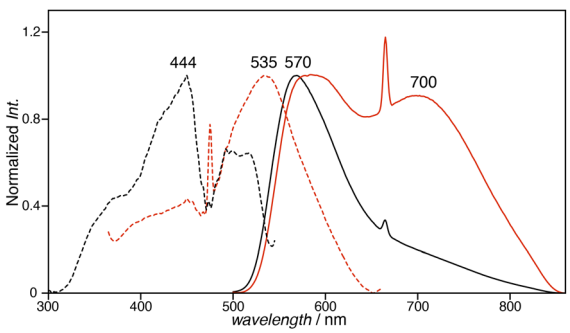

Fig. 2 Solid-state excitation (dashed lines) and emission (solid lines) spectra[58] of $\mathbf{1}_{\mathbf{unground}}$ (black lines, $\lambda_{ex} = 444$ nm, $\lambda_{em} = 568$ nm) and $\mathbf{1}_{\mathbf{ground}}$ (red lines, $\lambda_{ex} = 444$ nm, $\lambda_{em} = 710$ nm) at room temperature.

Mechanisms of the mechanochromic behavior

To detail the mechano-responsive color change, the shear stress was applied to $\mathbf{1}_{\mathbf{unground}}$. The powder of $\mathbf{1}_{\mathbf{unground}}$ was placed on the lattice-grooved plate and subjected to the shear stress by the lattice-grooved plate jig of 12 mm in diameter. Under the normal force FN of 49.2 ± 0.1 N, by applying the strain of 100% for the sample thickness of 0.136 mm, the resultant shear stress of 91.7 ± 0.7 kPa was given to the sample at a rotational frequency of 1 Hz for 10 min (MCR-302 Anton Paar Inc.). The resulting powder displayed a relatively weak MMLCT band, leading to an inference that the pressing forces within the grinding process primarily contributed to the emission color change of **1** (Fig. S3†).

The role of the TEG chains in the mechanochromic behavior was established by a combination of infrared (IR) spectroscopy and density functional theory (DFT) calculations. The IR spectra of $\mathbf{1}_{\mathbf{unground}}$ and $\mathbf{1}_{\mathbf{ground}}$ were recorded using a JASCO J-1500 spectrometer with an attenuated total reflection (ATR) accessory. $\mathbf{1}_{\mathbf{unground}}$ showed characteristic IR bands at 764 and 1102 cm^{-1} (Fig. 3a, black line). Mechanical grinding resulted in the low-wavenumber shift of the two characteristic peaks to 761 and 1097 cm^{-1}, respectively (Fig. 3a, red line). To characterize these bands and their shifts, DFT calculations of monomeric **M1** and dimeric **M1**·**M1**[59] were performed at the B3LYP/Lanl2DZ computational level using the 6-31G(d) basis set[60] (Fig. 3b–d, S6, S7, Tables S1 and S2†). The raw calculation data were processed using a scale factor of 0.9614 for B3LYP/6-31G(d).[61] Considering that $\mathbf{1}_{\mathbf{ground}}$ was densely packed in the solid state to generate intermolecular Pt–Pt interactions, dimeric **M1**·**M1** should be suitable for estimating the electric structure of $\mathbf{1}_{\mathbf{ground}}$. In contrast, monomeric **1** is a good model for estimating the electric structure of $\mathbf{1}_{\mathbf{unground}}$ because luminescence measurements of $\mathbf{1}_{\mathbf{unground}}$ provided no evidence of Pt–Pt interactions. The calculated IR spectrum of monomeric **M1** indicated that the CH out-of-plane bending vibration of the phenylbipyridine ligand moiety displayed a band at 763 cm^{-1}, which is in good agreement with the experimentally observed band at 764 cm^{-1} ($\mathbf{1}_{\mathbf{unground}}$). Calculations of dimeric **M1**·**M1** revealed that the CH out-of-plane bending vibration band emerged in the low-wavenumber region compared to that of monomeric **M1**. A low-wavenumber shift was experimentally observed upon grinding **1**; thus, this low-wavenumber shift supports the inference that the packing structure of $\mathbf{1}_{\mathbf{ground}}$ is more condensed than that of $\mathbf{1}_{\mathbf{unground}}$, which permits intermolecular Pt–Pt interactions. Based on the calculations, the bands at 1102 cm^{-1} ($\mathbf{1}_{\mathbf{unground}}$) and 1097 cm^{-1} ($\mathbf{1}_{\mathbf{ground}}$) correspond to C–O–C asymmetric vibrations.[62] The band (≈1100 cm^{-1}) was not observed in the IR spectrum of **2**, leading to an inference that the bands were derived from C–O–C asymmetric vibrations of the TEG chains (Fig. S4†). Thus, the low-wavenumber shift upon grinding suggests that mechanical grinding induced a conformational change in the TEG chains

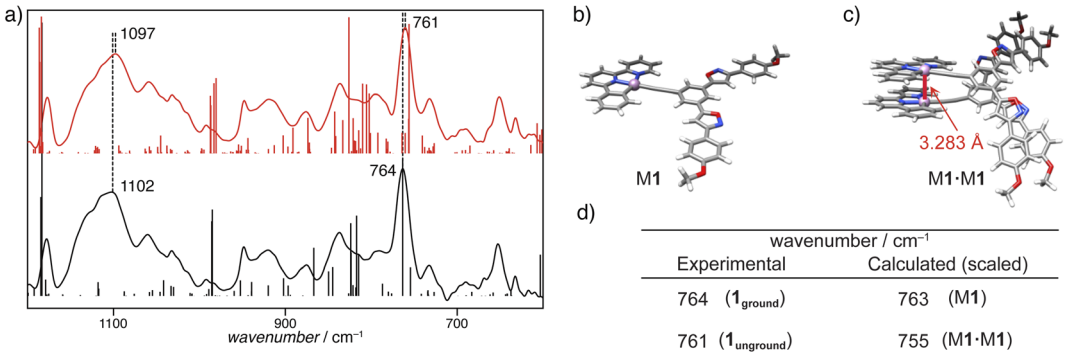

wavenumber / cm^{-1}	
Experimental	Calculated (scaled)
764 ($\mathbf{1}_{ground}$)	763 (M1)
761 ($\mathbf{1}_{unground}$)	755 (M1·M1)

Fig. 3 (a) Observed IR spectra of $\mathbf{1}_{unground}$ (black line) and $\mathbf{1}_{ground}$ (red line) and DFT-calculated IR intensities of monomeric **M1** (black bar) and dimeric **M1**·**M1** (red bar). The calculated frequencies were scaled by 0.9614. The intensities are listed in Tables S1 and S2.† Calculated structures of (b) monomeric **M1** and (c) dimeric **M1**·**M1** optimized at the B3LYP/Lanl2DZ computational level with the 6-31G(d) basis set for the estimation of the vibrational mode shown in panel a and Tables S1 and S2.† (d) Comparison of the experimental and calculated (scaled) vibrational wavenumbers (cm^{-1}) of **1** and **M1** (CH out-of-plane bending mode).

from a chain-folded conformation to a fully or partially extended conformation.[62]

The phase information of **1** was obtained using solid-phase powder X-ray diffraction (PXRD). $\mathbf{1}_{unground}$ exhibited scattering in the small-angle region ($2\theta < 10°$), suggesting the presence of large-scale heterogeneous structures. The broad scattering at approximately $2\theta = 23°$ indicates the amorphous nature of $\mathbf{1}_{unground}$ (Fig. 4, black line). Grinding resulted in minimal changes[63] in the PXRD pattern ($\mathbf{1}_{ground}$) (Fig. 4, red line), which clearly indicated that mechanical grinding did not induce a phase transition of **1** in the solid state. These results were obtained for a three-dimensionally aggregated bulk solid of **1**; thus, it can be concluded that the mechanochromic behavior of **1** was driven by a change in the molecular arrangement within the amorphous phase.

The thermal behaviors of $\mathbf{1}_{unground}$ and $\mathbf{1}_{ground}$ were studied using differential scanning calorimetry (DSC), providing insights into the mechanism of color change upon grinding. $\mathbf{1}_{unground}$ displayed endothermic peaks at 69.5, 79.3, and 159.4 °C in the heating run (Fig. 5, black line), whereas the DSC trace of $\mathbf{1}_{ground}$ showed endothermic peaks at 75.8, 94.0, 156.8, and 165.4 °C in the heating run (Fig. 5, red line). In addition to the endothermic peaks, exothermic peaks were observed at 118.7 °C and 121.2 °C in the bulk solid specimens of $\mathbf{1}_{unground}$ and $\mathbf{1}_{ground}$, respectively. The equilibrium melting point (T_m) of polyethylene glycol (PEG) is known to be at approximately 60 °C.[64] Accordingly, the broad endothermic peaks of $\mathbf{1}_{unground}$ and $\mathbf{1}_{ground}$ observed between 65 and 95 °C can be attributed to the changes in the molecular arrangement of **1** in the bulk solid derived from melting of the TEG chains. Moreover, the broad peak between 65 and 95 °C of $\mathbf{1}_{ground}$ was more intense compared with that of $\mathbf{1}_{unground}$, which indicates that the TEG chains of $\mathbf{1}_{ground}$ were packed with higher affinity, forming conformationally rigid packing structures in the solid state. The exothermic peak at approximately 120 °C can be rationalized by the reorientation of the TEG chains. The endothermic peak at 159.4 °C in $\mathbf{1}_{unground}$ corresponds to the T_m of **1**. Additionally, two separate endothermic peaks were observed at 156.9 °C and 165.2 °C. A split DSC peak such as this corresponding to T_m is caused by the reorientation of the molecular arrangement in bulk. In the case of $\mathbf{1}_{gournd}$, one corresponds to the T_m of **1** and the other is derived from the dissociation of intermolecular Pt–Pt interactions within the bulk solid of $\mathbf{1}_{ground}$. This consideration is supported by the experimental results shown in Fig. 2. No Pt–Pt interactions were evidenced in $\mathbf{1}_{unground}$, whereas $\mathbf{1}_{ground}$ was densely packed through intermolecular Pt–Pt interactions. Moreover, $\mathbf{2}_{ground}$ did not show the endothermic

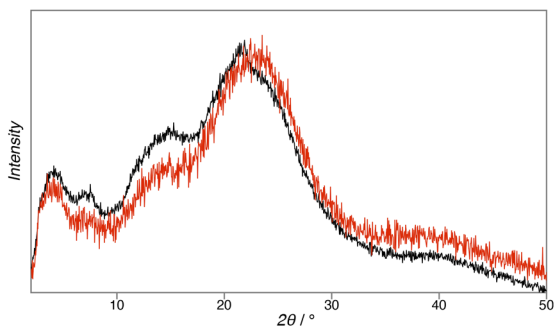

Fig. 4 Powder X-ray diffraction (PXRD) patterns of $\mathbf{1}_{unground}$ (black line) and $\mathbf{1}_{ground}$ (red line).

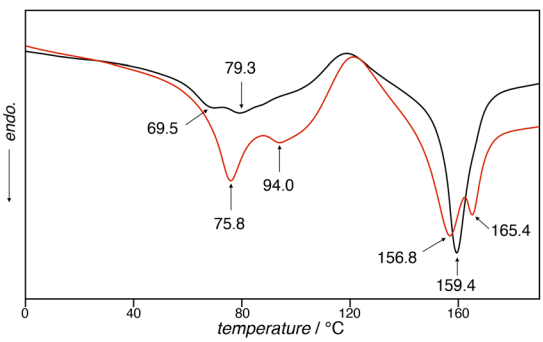

Fig. 5 DSC curves of $\mathbf{1}_{unground}$ (black line) and $\mathbf{1}_{ground}$ (red line) showing the 1st heating run at a heating rate of 15 °C min^{-1}.

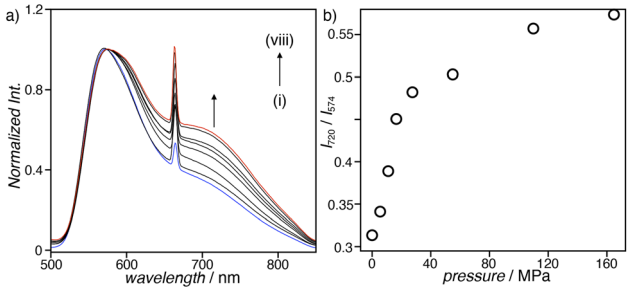

Fig. 6 (a) Changes in the emission spectra[58] of **1** (λ_{ex} = 444 nm) in the solid state. The pressures applied are: (i)–(viii) 0, 5.5, 11, 16, 27, 55, 110, and 165 MPa, respectively. The blue and red lines represent the first point and the last point of the measurement, respectively. (b) Plot of the normalized emission intensity of **1** at 720 nm against the pressure applied, showing the continuous changes in the emission intensity upon pressing.

peak at approximately 160 °C characteristic of the cleavage of Pt–Pt interactions, indicating that grounding did not induce the formation of Pt–Pt interactions within the powder **2** in bulk (Fig. S5†). These results indicates that the color change of **1** was driven by the conformational changes of the TEG chains and square-planar platinum moiety, as well as the reorientation of the molecular arrangement in bulk by the application of mechanical forces.

Visualization of the mechanical forces

The mechano-responsive nature of **1** allows the quantification of mechanical forces using a luminescence spectrometer. The MMLCT emission band grew upon the application of pressure (Fig. 6). The plot of the intensity of the MMLCT emission (720 nm) against pressure showed a continuous increase in the emission intensity, which can be read using a luminescence spectrometer. The steep increase in the emission intensity in the pressure range 0–20 MPa was gradually saturated when the total pressure reached approximately 80 MPa. This observation highlights the potential of **1** as a pressure sensor in the pressure range 0–20 MPa.

Conclusions

In summary, we demonstrated that a platinum(II) complex possessing TEG chains **1** showed a significant change in absorption and emission colors upon the application of mechanical forces. Color changes were found to be driven by a combination of conformational changes within the molecule and changes in the molecular arrangement in bulk. PXRD measurements confirmed that a mechano-responsive color change occurred in the amorphous phase. Moreover, luminescence spectroscopy, IR spectroscopy, and DSC measurements revealed that the conformational flexibility of the TEG chains imparted mechanochromic features to the Pt complex. Many mechanochromic molecules contain oligo-ethylene oxide chains within the molecular skeleton;[65–68] thus, our detailed studies elucidated the mechano-responsive color transformation with the participation of TEG chains in bulk. This work underscores the potential benefits of both TEG chains and square-planar platinum complexes for the creation of mechanochromic materials capable of quantitatively visualizing mechanical forces. These findings are expected to serve as a design guide for luminophore/dye-based mechanical force sensors.

Data availability

The data that supports the findings of this study are available in the ESI† of this article.

Author contributions

The manuscript was written through contributions of all authors. All authors have given approval to the final version of the manuscript.

Conflicts of interest

There are no conflicts to declare.

Acknowledgements

The authors are grateful to Ms Naomi Kawata and Ms Tomoko Amimoto of the Natural Science Center for Basic Research Development (N-BARD) at Hiroshima University for facilitating the PXRD experiments and HRMS measurements, respectively. The authors thank Mr Motonari Kobayashi of the Department of Instrumental Analysis & Cryogenics Division of Instrumental Analysis at Okayama University for facilitating the elemental analysis. This work was supported by JSPS KAKENHI Grants-in-Aid for Transformative Research Areas, "Condensed Conjugation" Grant Number JP21H05491 and "Materials Science of Meso-Hierarchy" Grant Number JP23H04873, Grants-in-Aid for Scientific Research (A) Grant Number JP21H04685, a Grant-in-Aid for Young Scientists Grant Number JP22K14727, and a Grant-in-Aid for JSPS Fellow JP23KJ1640. We acknowledge the support of KEIRIN JKA (Grant Number 2023M-419). Funding from the Hosokawa Powder Technology Foundation, Kumagai Foundation for Science and Technology, Mukai Science Technology Foundation, Shorai Foundation for Science and Technology, Amano Institute of Technology, and Old River Foundation is gratefully acknowledged.

Notes and references

1 Y. Sagara and T. Kato, *Nat. Chem.*, 2009, **1**, 605–610.
2 F. Ciardelli, G. Ruggeri and A. Pucci, *Chem. Soc. Rev.*, 2013, **42**, 857–870.
3 Y. Sagara, S. Yamane, M. Mitani, C. Weder and T. Kato, *Adv. Mater.*, 2016, **28**, 1073–1095.
4 P. Xue, J. Ding, P. Wang and R. Lu, *J. Phys. Chem. C*, 2016, **4**, 6688–6706.
5 G. Chen and W. Hong, *Adv. Opt. Mater.*, 2020, **8**, 2000984.
6 Y. Sun, Z. Lei and H. Ma, *J. Phys. Chem. C*, 2022, **10**, 14834–14867.

7 Y.-A. Lee and R. Eisenberg, *J. Am. Chem. Soc.*, 2003, **125**, 7778–7779.
8 Y. Sagara, T. Mutai, I. Yoshikawa and K. Araki, *J. Am. Chem. Soc.*, 2007, **129**, 1520–1521.
9 H. Ito, T. Saito, N. Oshima, N. Kitamura, S. Ishizaka, Y. Hinatsu, M. Wakeshima, M. Kato, K. Tsuge and M. Sawamura, *J. Am. Chem. Soc.*, 2008, **130**, 10044–10045.
10 T. Abe, T. Itakura, N. Ikeda and K. Shinozaki, *Dalton Trans.*, 2009, 711–715.
11 S.-J. Yoon, J. W. Chung, J. Gierschner, K. S. Kim, M.-G. Choi, D. Kim and S. Y. Park, *J. Am. Chem. Soc.*, 2010, **132**, 13675–13683.
12 G. Zhang, J. Lu, M. Sabat and C. L. Fraser, *J. Am. Chem. Soc.*, 2010, **132**, 2160–2162.
13 H. Ito, M. Muromoto, S. Kurenuma, S. Ishizaka, N. Kitamura, H. Sato and T. Seki, *Nat. Commun.*, 2013, **4**, 2009.
14 Q. Benito, X. F. Le Goff, S. Maron, A. Fargues, A. Garcia, C. Martineau, F. Taulelle, S. Kahlal, T. Gacoin, J.-P. Boilot and S. Perruchas, *J. Am. Chem. Soc.*, 2014, **136**, 11311–11320.
15 P. Galer, R. C. Korošec, M. Vidmar and B. Šket, *J. Am. Chem. Soc.*, 2014, **136**, 7383–7394.
16 M. Krikorian, S. Liu and T. M. Swager, *J. Am. Chem. Soc.*, 2014, **136**, 2952–2955.
17 Y. Lv, Y. Liu, X. Ye, G. Liu and X. Tao, *CrystEngComm*, 2015, **17**, 526–531.
18 X.-P. Zhang, J.-F. Mei, J.-C. Lai, C.-H. Li and X.-Z. You, *J. Phys. Chem. C*, 2015, **3**, 2350–2357.
19 K. Ohno, S. Yamaguchi, A. Nagasawa and T. Fujihara, *Dalton Trans.*, 2016, **45**, 5492–5503.
20 A. Lavrenova, D. W. R. Balkenende, Y. Sagara, S. Schrettl, Y. C. Simon and C. Weder, *J. Am. Chem. Soc.*, 2017, **139**, 4302–4305.
21 W. Yang, C. Liu, S. Lu, J. Du, Q. Gao, R. Zhang, Y. Liu and C. Yang, *J. Phys. Chem. C*, 2018, **6**, 290–298.
22 F. Khan, M. Mahmoudi, P. K. Gupta, D. Volyniuk, J. V. Grazulevicius and R. Misra, *J. Phys. Chem. C*, 2023, **127**, 1643–1654.
23 Z. Chi, X. Zhang, B. Xu, X. Zhou, C. Ma, Y. Zhang, S. Liu and J. Xu, *Chem. Soc. Rev.*, 2012, **41**, 3878–3896.
24 Y. Xiong, J. Huang, Y. Liu, B. Xiao, B. Xu, Z. Zhao and B. Z. Tang, *J. Phys. Chem. C*, 2020, **8**, 2460–2466.
25 K. Ogumi, K. Nagata, Y. Takimoto, K. Mishiba and Y. Matsuo, *J. Phys. Chem. C*, 2022, **10**, 11181–11186.
26 S. Thazhathethil, T. Muramatsu, N. Tamaoki, C. Weder and Y. Sagara, *Angew. Chem., Int. Ed.*, 2022, **61**, e202209225.
27 V. C. Ritter, S. M. McDonald, A. V. Dobrynin, S. L. Craig and M. L. Becker, *Adv. Mater.*, 2023, **35**, 2302163.
28 X. Yang, N. Li, B. Wang, P. Chen, S. Ma, Y. Deng, S. Lü and Y. Tang, *Angew. Chem., Int. Ed.*, 2025, **64**, e202419114.
29 Y. Zhu, M. Pan, L. Ma and Y. Wang, *Chem. Eng. J.*, 2025, **505**, 159245.
30 J. Brooks, Y. Babayan, S. Lamansky, P. I. Djurovich, I. Tsyba, R. Bau and M. E. Thompson, *Inorg. Chem.*, 2002, **41**, 3055–3066.
31 V. W.-W. Yam, V. K.-M. Au and S. Y.-L. Leung, *Chem. Rev.*, 2015, **115**, 7589–7728.
32 M. Nakagaki, S. Aono, M. Kato and S. Sakaki, *J. Phys. Chem. C*, 2020, **124**, 10453–10461.
33 M. Yoshida and M. Kato, *Coord. Chem. Rev.*, 2018, **355**, 101–115.
34 D. Saito, T. Ogawa, M. Yoshida, J. Takayama, S. Hiura, A. Murayama, A. Kobayashi and M. Kato, *Angew. Chem., Int. Ed.*, 2020, **59**, 18723–18730.
35 J. Ni, Y.-H. Wu, X. Zhang, B. Li, L.-Y. Zhang and Z.-N. Chen, *Inorg. Chem.*, 2009, **48**, 10202–10210.
36 J. Ni, X. Zhang, N. Qiu, Y.-H. Wu, L.-Y. Zhang, J. Zhang and Z.-N. Chen, *Inorg. Chem.*, 2011, **50**, 9090–9096.
37 S. J. Choi, J. Kuwabara, Y. Nishimura, T. Arai and T. Kanbara, *Chem. Lett.*, 2012, **41**, 65–67.
38 X. Zhang, J.-Y. Wang, J. Ni, L.-Y. Zhang and Z.-N. Chen, *Inorg. Chem.*, 2012, **51**, 5569–5579.
39 X. Zhang, Z. Chi, Y. Zhang, S. Liu and J. Xu, *J. Phys. Chem. C*, 2013, **1**, 3376–3390.
40 A. Han, P. Du, Z. Sun, H. Wu, H. Jia, R. Zhang, Z. Liang, R. Cao and R. Eisenberg, *Inorg. Chem.*, 2014, **53**, 3338–3344.
41 C.-J. Lin, Y.-H. Liu, S.-M. Peng, T. Shinmyozu and J.-S. Yang, *Inorg. Chem.*, 2017, **56**, 4978–4989.
42 L. Liu, X. Wang, N. Wang, T. Peng and S. Wang, *Angew. Chem., Int. Ed.*, 2017, **56**, 9160–9164.
43 C.-Y. Lien, Y.-F. Hsu, Y.-H. Liu, S.-M. Peng, T. Shinmyozu and J.-S. Yang, *Inorg. Chem.*, 2020, **59**, 11584–11594.
44 J. Ni, G. Liu, M. Su, W. Zheng and J. Zhang, *Dyes Pigm.*, 2020, **180**, 108451.
45 Q.-Y. Yang, H.-H. Zhang, X.-W. Qi, S.-S. Sun, D.-S. Zhang, L.-Z. Han, X.-P. Zhang and Z.-F. Shi, *Dalton Trans.*, 2021, **50**, 8938–8946.
46 H.-H. Zhang, Q.-Y. Yang, X.-W. Qi, S.-S. Sun, B.-S. Li, D.-S. Zhang, X.-P. Zhang and Z.-F. Shi, *Inorg. Chim. Acta*, 2021, **523**, 120411.
47 D. Gómez de Segura, E. Lalinde and M. T. Moreno, *Inorg. Chem.*, 2022, **61**, 20043–20056.
48 Q.-Z. Yuan, F.-S. Wan, T.-T. Shen and D.-K. Cao, *RSC Adv.*, 2022, **12**, 148–153.
49 H.-H. Zhang, S.-X. Wu, Y.-Q. Wang, T.-G. Xie, S.-S. Sun, Y.-L. Liu, L.-Z. Han, X.-P. Zhang and Z.-F. Shi, *Dyes Pigm.*, 2022, **197**, 109857.
50 H. Sogawa, M. Abe, R. Shintani, T. Sotani, K. Tabaru, T. Watanabe, Y. Obora and F. Sanda, *Polym. J.*, 2023, **55**, 1119–1128.
51 B.-C. Tzeng, C.-C. Liao, P.-Y. Jung, S.-Y. Chen, B.-J. Sun, W.-C. Cheng, A. H. H. Chang and G.-H. Lee, *Inorg. Chem.*, 2023, **62**, 916–929.
52 T. Ikeda, M. Takayama, J. Kumar, T. Kawai and T. Haino, *Dalton Trans.*, 2015, **44**, 13156–13162.
53 T. Ikeda and T. Haino, *Polymer*, 2017, **128**, 243–256.
54 T. Haino and T. Hirao, *Chem. Lett.*, 2020, **49**, 574–584.
55 T. Hirao, H. Tsukamoto, T. Ikeda and T. Haino, *Chem. Commun.*, 2020, **56**, 1137–1140.
56 M. Yoshida, T. Hirao and T. Haino, *Org. Biomol. Chem.*, 2021, **19**, 5303–5311.
57 M. Yoshida, T. Hirao and T. Haino, *Chem. Commun.*, 2022, **58**, 8356–8359.

58 The spike peaks found in the emission and excited spectra arise from excitation light.
59 Dimeric **M1**·**M1** in a head-to-tail stacking arrangement prevents the formation of intermolecular Pt–Pt interactions; thus, we studied with dimeric **M1**·**M1** in a head-to-head stacking arrangement shown in Fig. 3c.
60 M. J. Frisch, G. W. Trucks, H. B. Schlegel, G. E. Scuseria, M. A. Robb, J. R. Cheeseman, G. Scalmani, V. Barone, G. A. Petersson, H. Nakatsuji, X. Li, M. Caricato, A. V. Marenich, J. Bloino, B. G. Janesko, R. Gomperts, B. Mennucci, H. P. Hratchian, J. V. Ortiz, A. F. Izmaylov, J. L. Sonnenberg, D. Williams-Young, F. Ding, F. Lipparini, F. Egidi, J. Goings, B. Peng, A. Petrone, T. Henderson, D. Ranasinghe, V. G. Zakrzewski, J. Gao, N. Rega, G. Zheng, W. Liang, M. Hada, M. Ehara, K. Toyota, R. Fukuda, J. Hasegawa, M. Ishida, T. Nakajima, Y. Honda, O. Kitao, H. Nakai, T. Vreven, K. Throssell, J. A. Montgomery Jr, J. E. Peralta, F. Ogliaro, M. J. Bearpark, J. J. Heyd, E. N. Brothers, K. N. Kudin, V. N. Staroverov, T. A. Keith, R. Kobayashi, J. Normand, K. Raghavachari, A. P. Rendell, J. C. Burant, S. S. Iyengar, J. Tomasi, M. Cossi, J. M. Millam, M. Klene, C. Adamo, R. Cammi, J. W. Ochterski, R. L. Martin, K. Morokuma, O. Farkas, J. B. Foresman and D. J. Fox, *Gaussian 16, Revision C.01*, Gaussian, Inc., Wallingford CT, 2016.
61 A. P. Scott and L. Radom, *J. Phys. Chem.*, 1996, **100**, 16502–16513.
62 J. J. Shephard, P. J. Bremer and A. J. McQuillan, *J. Phys. Chem. B*, 2009, **113**, 14229–14238.
63 The grinding induced a slight wide-angle shift of the peak top of $2\theta = 23°$ and a decrease in intensity of diffraction around at $2\theta = 14°$. The slight changes in the diffraction pattern appear to be reorientation of molecular arrangement of **1** to form densely packed structures in bulk.
64 T. Jayaramudu, G. M. Raghavendra, K. Varaprasad, G. V. S. Reddy, A. B. Reddy, K. Sudhakar and E. R. Sadiku, *J. Appl. Polym. Sci.*, 2016, **133**, 43027.
65 S. Yagai, T. Seki, H. Aonuma, K. Kawaguchi, T. Karatsu, T. Okura, A. Sakon, H. Uekusa and H. Ito, *Chem. Mater.*, 2016, **28**, 234–241.
66 J. Zessin, M. Schnepf, U. Oertel, T. Beryozkina, T. A. F. König, A. Fery, M. Mertig and A. Kiriy, *Adv. Opt. Mater.*, 2020, **8**, 1901410.
67 H. Sakai, K. Nonaka, R. Hayasaka, S. Thazhathethil, Y. Sagara and T. Hasobe, *Chem. Commun.*, 2024, **60**, 4084–4087.
68 S. Thazhathethil, F. S. Thuluvanchery, S. Shimizu, I. Scarlat, J. M. Clough, C. Weder and Y. Sagara, *J. Phys. Chem. C*, 2024, **12**, 6170–6176.